

Impact of the circulation on sapropel formation in the eastern Mediterranean

Kevin Stratford

Department of Meteorology, University of Edinburgh, Edinburgh, United Kingdom

Richard G. Williams

Oceanography Laboratories, Department of Earth Sciences, University of Liverpool, Liverpool, United Kingdom

Paul G. Myers

Department of Physics and Physical Oceanography, Memorial University of Newfoundland, St. John's, Canada

Abstract. The role of the thermohaline circulation in controlling export production, oxygenation of deep waters, and hence possible sapropel formation in the eastern Mediterranean is examined using a simple nutrient-cycling model. The model is driven by velocity fields from a general circulation model and receives fluxes of nutrient from river run-off and atmospheric deposition. The model is used to study three scenarios: a strong anti-estuarine circulation, a weakened anti-estuarine circulation, and a weak estuarine circulation. Nutrient transports, ventilation of oxygen, and deposition of organic matter are investigated in each case. With a present-day circulation the model provides reasonable agreement with observed phosphate and oxygen profiles and for export production. With the weakened anti-estuarine circulation, consistent with surface salinity reconstructions for the most recent sapropel S_1 , there is a modest increase in export production and reduced ventilation leading to anoxia in intermediate and deep waters. Sapropel formation is possible near the coastal margins, particularly if there is enhanced river run-off. With an estuarine circulation, there is significant increase in export production in addition to anoxia below a shallow winter mixed layer. While both the latter circulations allow sapropel formation in the model, the estuarine case is distinguished by higher organic carbon deposition and anoxia in the near-surface waters.

1. Introduction

Organic carbon-rich sediments, or sapropels, have been deposited episodically in the eastern Mediterranean and provide important evidence for past changes in climate (for a review, see *Rohling* [1994]). Sapropels are formed by a combination of two factors: increased biological production associated with a higher nutrient supply to the euphotic zone and increased organic preservation in the sediments owing to decreased ventilation and suboxic deep waters. An increase in the nutrient supply may be achieved by increased surface fluxes (from river and atmosphere) or changes in the upwelling of nutrient-rich, deep waters. The existence of these different mechanisms has meant that the relative importance of the circulation in sapropel formation is the subject of an on-going debate. Of particular interest is the ex-

tent to which a change in buoyancy forcing, associated with a different climatic state, might have altered the overturning circulation of the eastern Mediterranean.

Sapropels with a high organic carbon content have been connected to a reversal of the present-day, anti-estuarine circulation [*Sarmiento et al.*, 1988; *Thunell and Williams*, 1989] and to surface waters being highly stratified [*Sancetta*, 1994; *Kemp et al.*, 1999]. In contrast, sapropels with relatively low organic carbon content (e.g., the most recent sapropel S_1) have been explained solely in terms of a weakening of the anti-estuarine circulation [*Rohling and Gieskes*, 1989; *Rohling*, 1994]. In this study, coupled physical and biogeochemical models are employed to understand the different processes affecting sapropel formation. This coupled approach highlights the combined, rather than separate, role of changes in stratification, ventilation, and overturning circulation brought about by changes in surface buoyancy forcing associated with different climates.

The study is undertaken as follows. A general circulation model (GCM) is employed to produce three differ-

Copyright 2000 by the American Geophysical Union.

Paper number 1999GB001157.
0886-6236/00/1999GB001157\$12.00

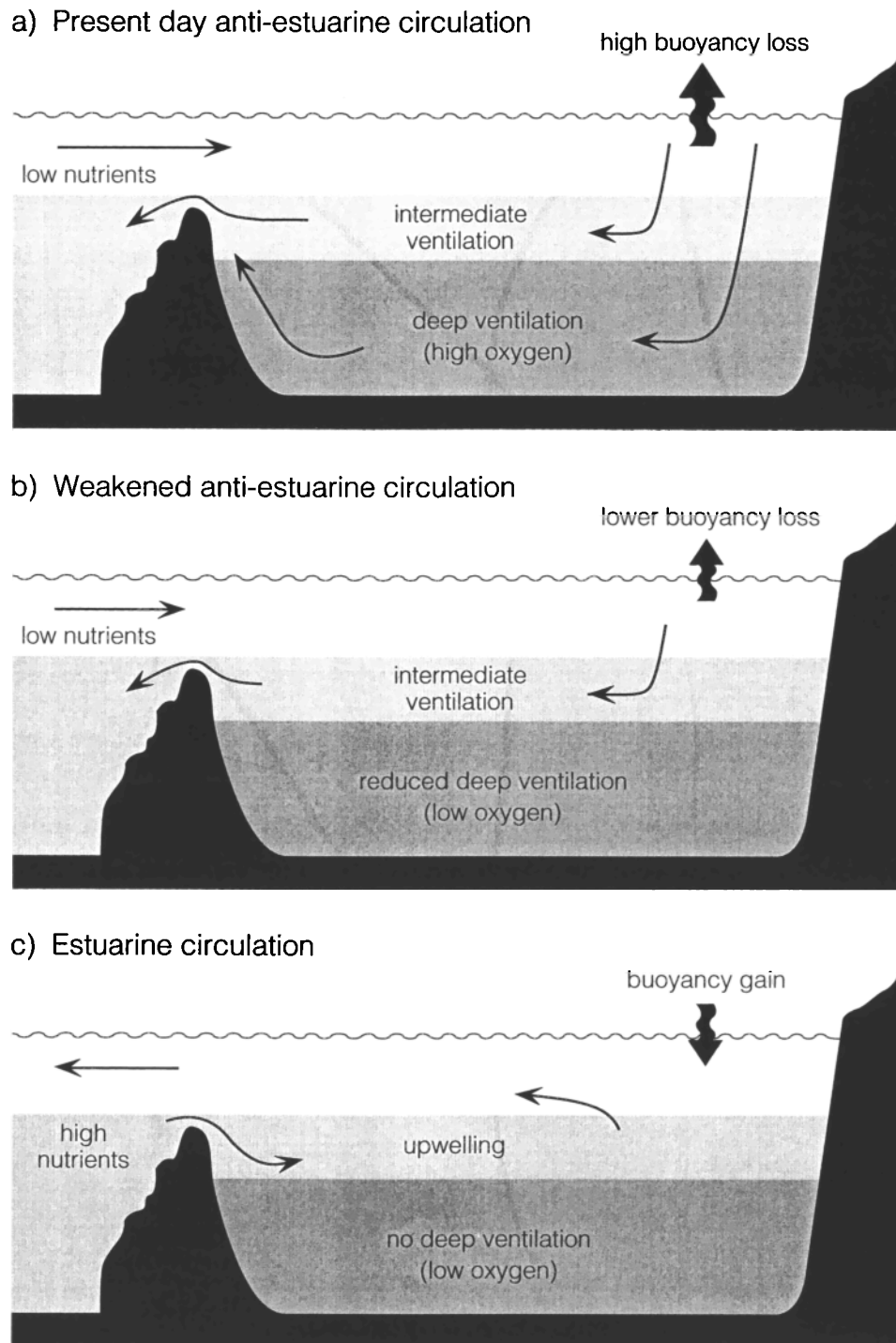


Figure 1. A schematic figure shows the sense of the circulation in the eastern Mediterranean. (a) The circulation is strongly anti-estuarine at present, driven by an intense buoyancy loss at the surface (largely evaporation). This is accompanied by strong deep water formation and an inflow of relatively fresh surface water with a low nutrient content. (b) A reduced surface buoyancy loss leads to shallower ventilation, while (c) a buoyancy gain leads to an estuarine (or “reversed”) circulation with an inflow of deeper, nutrient-enriched water.

ent thermohaline circulations in the eastern Mediterranean basin as illustrated in Figure 1: the present-day strong anti-estuarine circulation, a weakened anti-estuarine circulation, and a weak estuarine circulation. The sense of the circulation in the GCM is controlled via the surface buoyancy (in particular, salinity) forcing. The simple nutrient-cycling model is then run in conjunction with the different circulations to assess their impact on modeled productivity (limited by phosphate) and the amount of organic material reaching the sea floor (controlled by deep water oxygen concentrations). The sensitivity of the model to higher external fluxes of nutrient is assessed for each circulation.

Section 2 examines the physical model and resultant circulations, which are used to drive the biogeochemical model described in section 3. The results of the biogeochemical model are presented in section 4. A discussion and short summary conclude.

2. Anti-estuarine and Estuarine Circulations

The present day Mediterranean suffers a net buoyancy loss which drives a strong anti-estuarine circulation, involving an inflow of Atlantic surface water and an outflow of denser Mediterranean water. (At present the sense of the circulation at Gibraltar is the same as that at Sicily.) The thermohaline circulation responds to changes in buoyancy forcing associated with changes in climate: for example, climatic conditions in the early Holocene period (10,000–6000 years ago) are thought to have been relatively warm and humid compared to the present day [Mangini and Schlosser, 1986], which would result in a decreased buoyancy loss and a weaker anti-estuarine circulation. Climatic conditions leading to a buoyancy gain would excite an estuarine circulation (Figure 1). Note that the eastern Mediterranean also exhibits an internal thermohaline circulation consisting of deep water sources in the Adriatic and/or the Aegean Seas [Roether et al., 1996]. Variability of this internal circulation is not considered in the present work. Here, three different thermohaline circulations in the eastern Mediterranean are modeled: the present-day anti-estuarine circulation based on observational data, a weakened anti-estuarine circulation

based on palaeoceanographic salinity reconstructions for the early Holocene after Myers et al. [1998], and a hypothetical estuarine circulation used as a comparison.

2.1. General Circulation Model

The basis for the present work is the primitive equation model described by Killworth et al. [1991], which has been adapted for the Mediterranean following Pinardi and Navarra [1993], Roussenov et al. [1995], and Haines and Wu [1995]. The model resolution is $1/4^\circ$, permitting the growth of baroclinic eddies, with 19 unevenly spaced levels in the vertical. The subgrid scale parametrization of Gent and McWilliams [1990] is used, along with a flux-limited advection scheme for tracers [Thuburn, 1996].

For each circulation, the model tracers are initialized with climatological temperature and salinity fields appropriate for the present day [Brasseur et al., 1996]. The buoyancy flux at the surface is imposed via a relaxation of both surface temperature and salinity [cf. Haney, 1971] to prescribed values. For the present day, the relaxation is to monthly values, again from climatology. The model for the weakened anti-estuarine circulation uses the same temperature values but a salinity reconstruction of the Holocene optimum period from Kallel et al. [1997] in which the surface salinities are typically 3 practical salinity units (psu) lower than the present-day values. Myers et al. [1998] have employed a number of different surface salinity reconstructions from palaeoceanographic data and found the resulting circulations to be similar and also find the impact of temperature to be negligible in this case. In order to generate an estuarine circulation, a reduction in the surface salinity of around 6 psu compared with the present day is imposed. This results in a net buoyancy gain and a weakly estuarine circulation in the eastern basin (see Table 1).

For each set of conditions, the GCM has been integrated for 120 years with wind data from the European Centre for Medium-range Weather Forecasts (ECMWF) appropriate for the present day. Climate models [e.g., Hewitt and Mitchell, 1998] are currently of too poor a resolution to provide wind forcing (or fluxes) suitable for the current study. A steady state is approached in both anti-estuarine cases, while the estuarine case is still evolving to some extent, suggesting heat and freshwater flux forcing [e.g., Myers and Haines, 2000] might be required to maintain a buoyancy gain for timescales much longer than 100 years in the current model.

2.2. Modeled Circulations

The thermohaline circulation in the model is clearly revealed by the zonal overturning stream function

$$\psi(x, z) = \int dy \int_{-H}^z dz' u(x, y, z'), \quad (1)$$

where u is the annual mean zonal velocity field and $H(x)$ is the maximum depth of the water column at each longitude.

Table 1. Approximate Model $E - P$ and Strait Fluxes

	$E - P, \text{ m yr}^{-1}$	Strait Flux, Sv
Present Day	0.7	0.7
Weak Anti-Estuarine	0.1	0.2
Weak Estuarine	-0.4	-0.1

Evaporation (E) minus precipitation (P) and Sicily strait flux (Sv or $10^6 \text{ m}^3 \text{ s}^{-1}$) diagnosed from the model for the three different circulations. The negative sign indicates that there is an excess of precipitation over evaporation, accompanied by an inflow of deep water at Sicily.

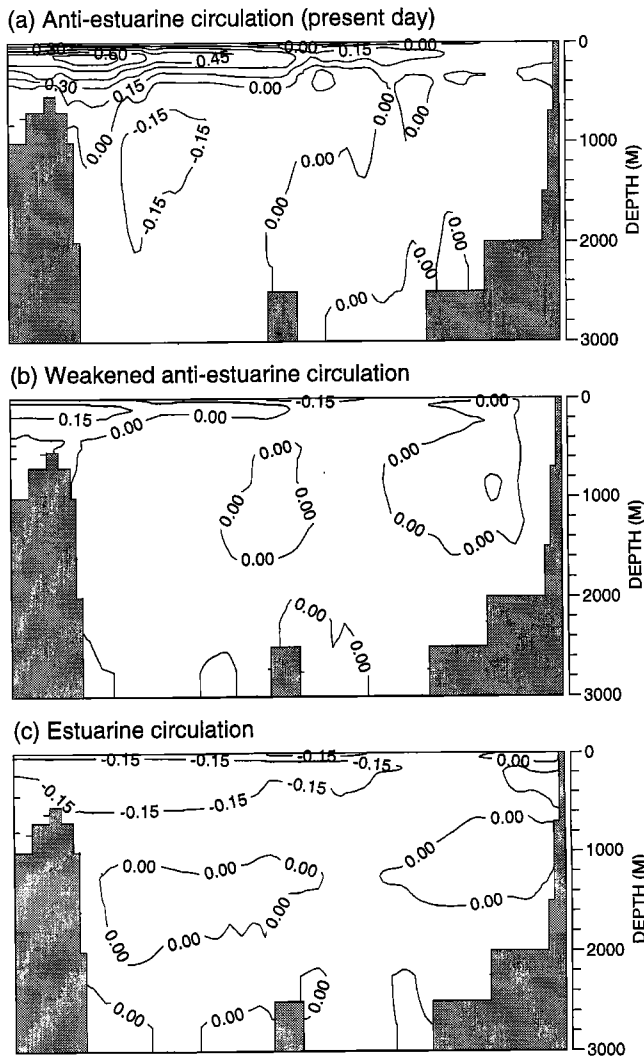


Figure 2. Zonal overturning stream functions for the eastern Mediterranean from three different GCM integrations: (a) the present day, (b) with surface salinity reduced by around 3 psu, and (c) surface salinity reduced by around 6 psu. The direction of the flow along streamlines is found by locating more positive values to the right of the flow. The contour interval is $0.15 \times 10^6 \text{ m}^3 \text{ s}^{-1}$ in all cases.

The stream function $\psi(x, z)$ in the eastern basin is shown in Figure 2. For the the present day model (Figure 2a) there is an anti-estuarine cell extending to 500 m, with eastward surface flow near Sicily and westward intermediate flow, accompanied by an internal cell with eastward flowing deep water. The weakened anti-estuarine case exhibits a shallower, weaker recirculation confined to 300 m overlying a stagnant abyss (Figure 2b). In the estuarine model, a shallow cell is seen at the surface with a surface outflow and intermediate depth inflow. The mean surface inflow at the Sicily Strait is 0.7 Sv for the present day and 0.2 Sv for the weakened anti-estuarine case (compensated by an equal deep outflow in the model). In the estuarine case, there is a mean surface outflow of 0.1 Sv, with corresponding deep inflow.

The mean salinity distributions corresponding to the differing circulations are shown along a transection through the eastern basin in Figure 3. The present day model (Figure 3a) forms eastern Mediterranean deep water in the Adriatic with salinity (38.6–38.7 psu) lower than that of the intermediate water. However, in the weakened anti-estuarine model, ventilation is limited to the upper 300–400 m (Figure 3b). A pronounced halocline is present, below which the salinity distribution is diffusively controlled. The situation in the model is more extreme in the estuarine case (Figure 3c), where there is a very strong halocline, with associated strong density stratification and no significant convection in the Adriatic.

The extent of convective overturning in the model reflects the different buoyancy forcing and is shown in Figure 4.

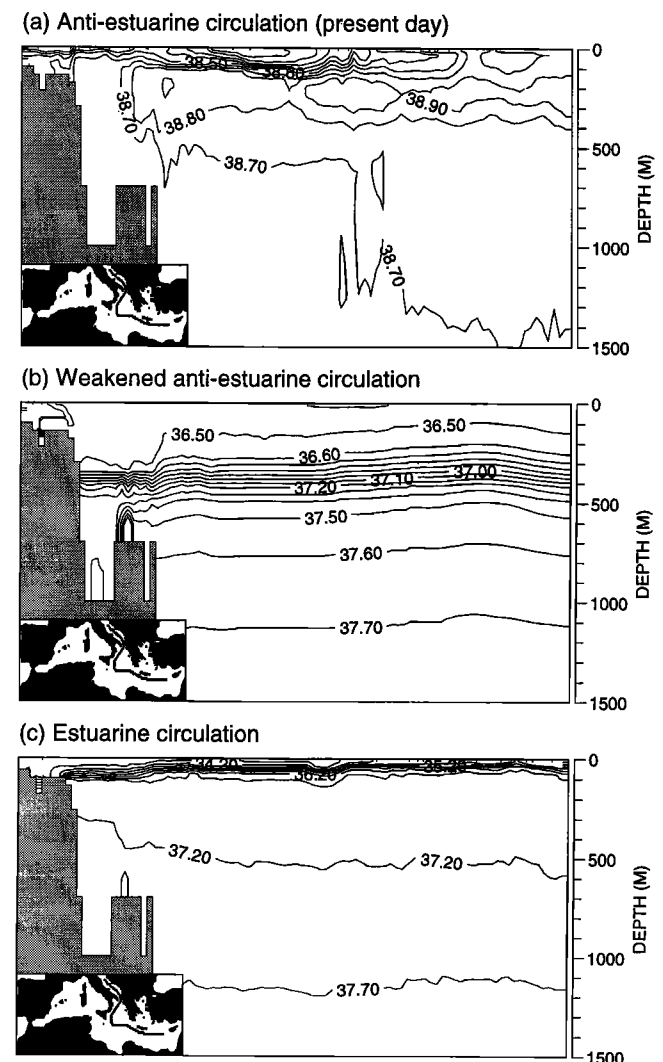


Figure 3. Vertical sections of annual average salinity (psu) along the path shown inset for the three different GCM configurations. (a) The present day model where deep water is well ventilated, (b) the weakened anti-estuarine case where shallow ventilation from the Adriatic occurs, and (c) the estuarine case where there is little or no ventilation are shown. Note the difference in contour interval (0.5 psu) in Figure 3c.

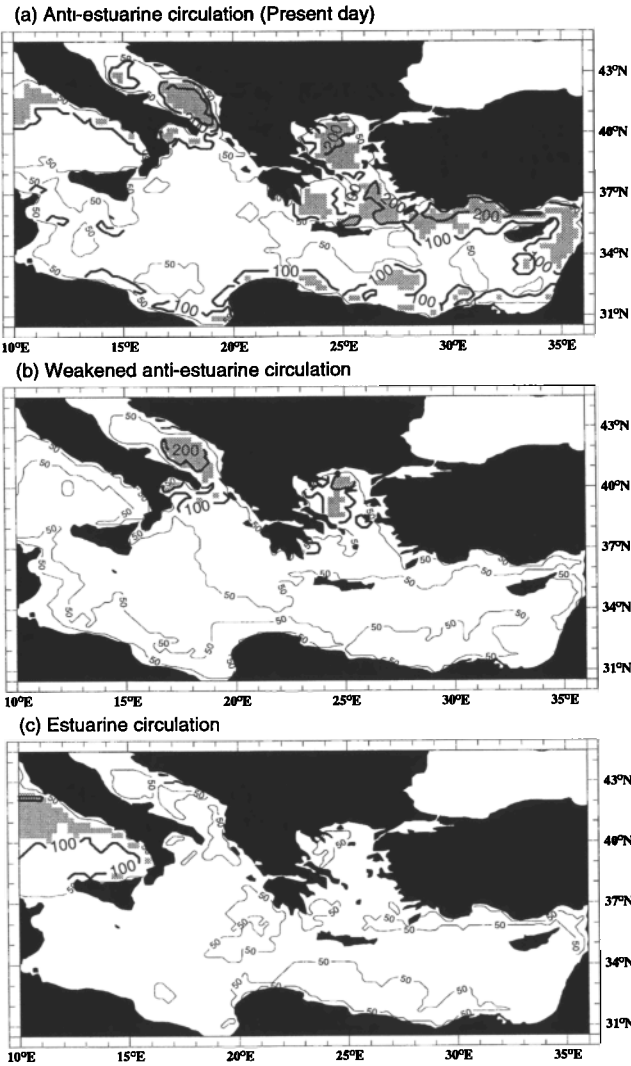


Figure 4. Maximum depth of winter convective overturning (m) in the the different GCM integrations. The shaded regions indicate convection beyond 100 m in the model. Note that there is significantly reduced convective overturning in the estuarine case, particularly in the Adriatic.

Strong winter mixing is observed in the present day integration, extending to 300–400 m in both the Adriatic and the Levant (Figure 4a), while shallower mixing is seen in the weakened anti-estuarine model (Figure 4b). In the estuarine case, where a buoyancy gain has been imposed, there is no convective mixing beyond 100 m in the eastern basin in the model.

3. Biogeochemical Model

A simplified nutrient-cycling model of the type described by *Najjar* [1990] [see, also, *Najjar et al.*, 1992] is now used to examine how changes in the circulation might influence export production via the supply of nutrients to the euphotic zone and the preservation of sinking organic matter which

is controlled by the oxygen content of the deep waters. The model is based on phosphate, which is observed to be the limiting nutrient in the eastern Mediterranean [*Berland et al.*, 1988; *Krom et al.*, 1991], while the cycling of oxygen is introduced via the remineralization of a detrital component, which represents the dead organic material falling through the water column. A simple representation of the effect of suboxic or anoxic conditions is included by letting the remineralization rate be a function of the local oxygen concentration. Furthermore, detritus is allowed to leave the system at the base of the water column in anoxic conditions to simulate sedimentation. A brief description of the model is given in sections 3.1 and 3.2, with details of the choice of parameters supplied in the appendix. Note that conversion to carbon units, where appropriate, is performed by assuming a C:P ratio of 100.

The biogeochemical model uses the same domain and resolution as the GCM (section 2.1) and is run “off-line” including a seasonal cycle for a perpetual year with 5 day resolution as described by *Stratford et al.* [1998]. Advection by the GCM velocity field again includes the effect of unresolved eddies via the *Gent and McWilliams* [1990] component of the advecting velocities, and a third-order forward-in-time flux-limited advection scheme is employed [*Stratford*, 1999] to prevent unphysical tracer values arising. The extent of convective overturning is also supplied with 5 day resolution.

3.1. Model Description

The model computes the time evolution of the concentrations of dissolved phosphate PO_4 , detrital material D , and dissolved oxygen O_2 , using the coupled equations:

$$\begin{aligned} [\text{PO}_4]_t &= -\nabla \cdot (\mathbf{u}[\text{PO}_4]) - \overline{(w'[\text{PO}_4])'}_z - \lambda[\text{PO}_4] + r[D], \\ [D]_t &= -\overline{(w'[D])'}_z + \lambda[\text{PO}_4] - r[D] - (w_s[D])_z, \\ [\text{O}_2]_t &= -\nabla \cdot (\mathbf{u}[\text{O}_2]) - \overline{(w'[\text{O}_2])'}_z - \mathcal{R}r[D]. \end{aligned} \quad (2)$$

The subscripts t and z refer to time and vertical derivatives, respectively, while the overbar represents a mean quantity and the dash represents a deviation from the mean. Equations (2) relate the time rate of change of each model quantity to a divergence of three-dimensional advective fluxes, the vertical divergence of turbulent fluxes, and a number of specific source and sink terms, respectively. Note that the detritus equation omits the three-dimensional advection, as the time scale for sinking is fast compared to that required for significant horizontal advection.

The light-limited uptake of phosphate in the surface layer is controlled by the rate λ , where $1/\lambda \sim 4$ weeks. Phosphate utilized is transferred to the detrital component, which is in turn remineralized to phosphate at a rate r . The detrital material falls through the water column with speed $w_s \sim 200 \text{ m d}^{-1}$. Oxygen is consumed during the remineralization of detritus, the total rate determined by the Redfield ratio \mathcal{R} [*Redfield et al.*, 1963] between oxygen and phosphorus in (2), \mathcal{R} is chosen to be 170 following *Takahashi et al.*

[1985]. Further coupling is incorporated locally by letting the remineralization rate decrease with decreasing oxygen concentration as described in the appendix.

3.2. Boundary Conditions

For phosphate, a flux boundary condition is used at the surface, allowing the total nutrient input to be specified explicitly. Sections 4.1 and 4.2 will describe two scenarios: first a low-nutrient flux based on estimates of a preanthropogenic state and second a high-nutrient flux which assumes an increase in river discharge of a factor of 3. This gives a river phosphate flux in the eastern basin of 30 mol s^{-1} for the low case and 90 mol s^{-1} in the high case. The river flux is distributed evenly between model points contiguous with the coastline. A constant atmospheric flux of 35 mol s^{-1} is distributed uniformly across the eastern basin. It should be noted that there is no seasonal cycle in the atmospheric and river phosphate flux.

Detritus reaching the sea-floor is instantaneously resuspended in the deepest model level, unless the local oxygen concentration drops below 0.06 mol m^{-3} [Rosenburg, 1980]. This represents the ability of the benthic community to recycle detrital material reaching the bottom, which is suppressed in suboxic or anoxic conditions.

The boundary conditions for oxygen are treated as a relaxation to a saturated value related to the surface temperature and salinity [Weiss, 1970] at a rate determined by a wind speed-dependent piston velocity [Liss and Merlivat, 1986]. The dominant factor here is the seasonal cycle in sea surface temperature, which is the same for each of the circulations. The initial conditions for all the integrations of the biogeochemical model consist of uniform values for the concentration of each component: $[\text{PO}_4] = 2 \times 10^{-4} \text{ mol m}^{-3}$, $[\text{D}] = 0$, and $[\text{O}_2] = 0.1 \text{ mol m}^{-3}$.

4. Model Results

4.1. Nutrient Fluxes and Anoxia

The nutrient-cycling model is now integrated using the different circulations in the eastern Mediterranean described in section 2.2: strong anti-estuarine (the present day), weakened anti-estuarine, and estuarine. Model runs of 1000 years are performed using low-nutrient inputs, which allows the intermediate circulations to approach equilibrium in all three cases. The surface nutrient input is then increased to the higher values, and the model is run on for a further 1000 years with each circulation to allow the deep circulation to approach equilibrium.

The mean concentrations of phosphate and oxygen in the eastern deep water (2500–3000 m) for the entire 2000 year period are shown in Figure 5. The present-day phosphate values exhibit little trend, while oxygen values remain high, even with increased nutrient input, owing to strong deep water ventilation (solid lines in Figure 5). There are more striking increases in phosphate concentration in the weakened

anti-estuarine and estuarine circulations (dashed and dotted lines in Figure 5, respectively), which are accompanied by decreases in deep oxygen concentration. Deep water nutrient concentrations do not reach a steady state after 2000 years, but deep water oxygen is depleted.

Figure 6 shows modeled profiles of phosphate and oxygen averaged over the eastern basin after 2000 years, which can be compared with profiles for the present day derived from a synthesis of observations [Krom *et al.*, 1991; Conkright *et al.*, 1994; Stratford *et al.*, 1998]. The modeled concentrations for the present day, anti-estuarine circulation are in reasonable agreement with the observations throughout the water column (allowing for the long period of high-nutrient input). Higher phosphate concentrations at depth for the weakened anti-estuarine and estuarine circulations reflect changes in the inflow and outflow at Sicily, while the extent of ventilation in the model means that there is suboxia below around 500 m in the weakened anti-estuarine circulation and below around 100 m in the estuarine case (on average). Note that the inflow conditions for the estuarine case are dependent upon the western basin, which also exhibits loss of ventilation and anoxia in the current model.

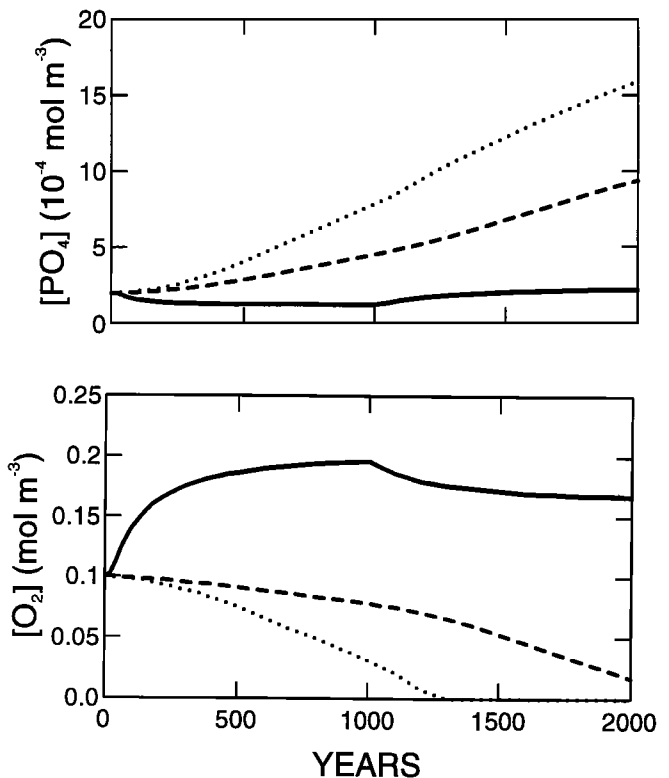


Figure 5. Times series of phosphate and oxygen values in the deep water (2500–3000 m) for the entire 2000 year integration. The solid line is the strong anti-estuarine circulation, the dashed line is the weakened anti-estuarine circulation, and the dotted line is the estuarine case. The discontinuity at 1000 years reflects the change from low to high external nutrient input regimes.

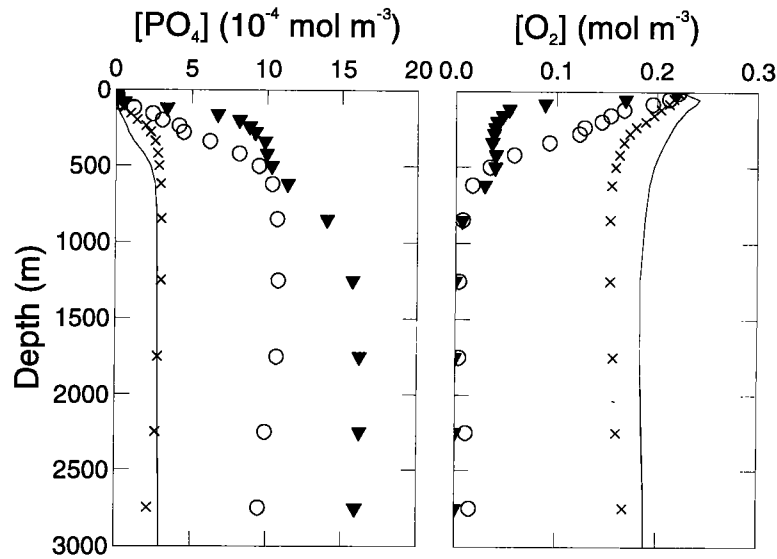


Figure 6. Mean profiles of phosphate and oxygen from the eastern basin for the three circulations at the end of 2000 years. The crosses are for the strong anti-estuarine model, the open circles are for the weakened anti-estuarine case, and the triangles are for the estuarine case. The continuous lines are a synthesis of observational data for the present day for comparison.

The phosphate budget for each circulation is shown in Table 2 in both high- and low-nutrient input cases. For the strong anti-estuarine circulation, the external inputs of phosphate balance the modeled outflux at Sicily, and there is no flux to the sea floor. For the weakened anti-estuarine circulation, there is a decreased nutrient outflux at Sicily owing to the reduced volume outflux of deep waters, even though there is an increase in phosphate concentration of the intermediate and deep waters. For the estuarine circulation, there is influx of both deep water and phosphate at Sicily into the eastern Mediterranean. Deep water anoxia in the weakened

anti-estuarine and estuarine cases allows a loss of nutrient (via detritus) to the sediment, while the budget is closed by increases in nutrient content of the deep waters (compare with Figure 5).

The vertical extent of the modeled anoxic region as a function of time for the weakened anti-estuarine and estuarine circulations is shown in Figure 7. The onset of anoxia, assumed here to be $0.06 \text{ mol O}_2 \text{ m}^{-3}$, occurs first at mid-depths in the model and then advances downward to 3000 m after 700 years and 1500 years for the estuarine and anti-estuarine circulations, respectively.

Table 2. Annual Phosphate Budget for the Model Circulations with Low- and High-Nutrient Input

	Fluxes, mol P s^{-1}			Net Gain, mol P s^{-1}	Export Production, mol P s^{-1}
	$R + A$	Net Inflow	To Sediment		
Strong Anti-Estuarine	65	-65	0	0	155
Weak Anti-Estuarine	65	-40	-20	5	185
Weak Estuarine	65	20	-25	60	355
Strong Anti-Estuarine	125	-120	0	5	300
Weak Anti-Estuarine	125	-75	-10	40	340
Weak Estuarine	125	35	-30	130	485

Phosphate fluxes from river and atmosphere ($R + A$) are balanced by the sum of the net inflow at Sicily, loss to the sediment, and net gain in concentration in the water column. In a steady state, there is no net gain of phosphate in the water column. Significant increases in export production in the model (mol P s^{-1}) are driven either by increased river and atmospheric sources or by an inflow of nutrients at Sicily associated with an estuarine circulation. Here the changes in the water column are inferred from conservation of total nutrient content and the budget is given to the nearest 5 mol P s^{-1} .

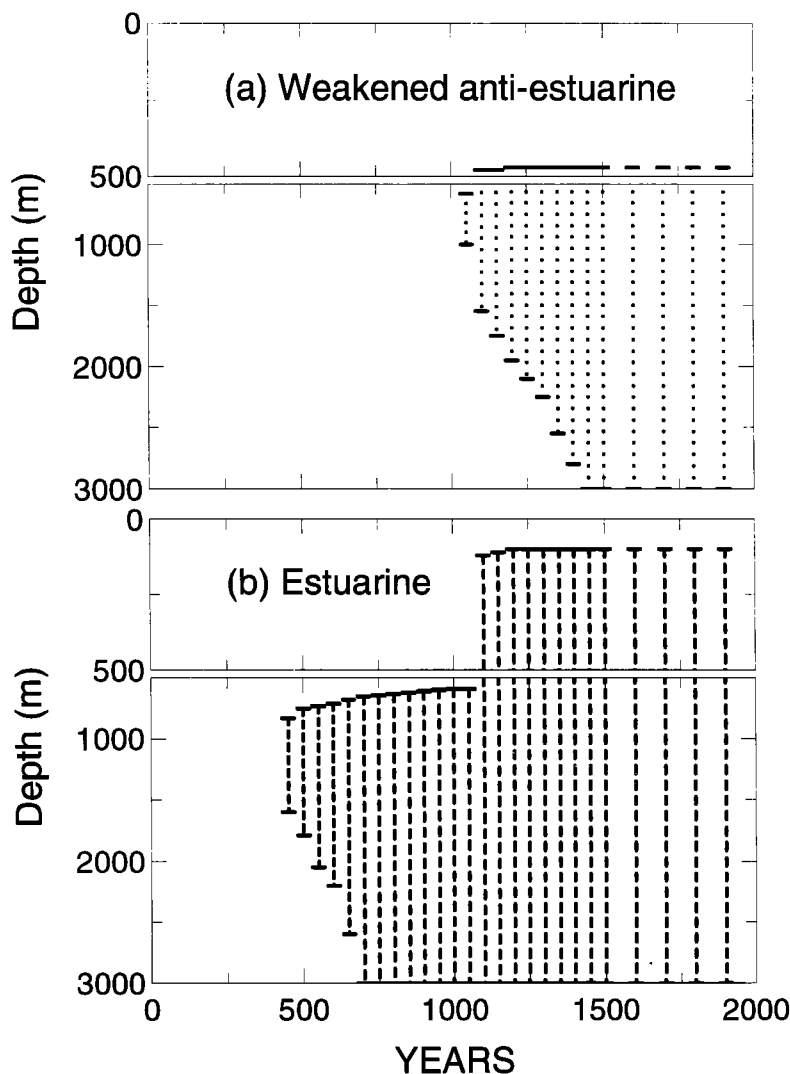


Figure 7. Time series showing the vertical extent of anoxia, defined by concentrations lower than $0.06 \text{ mol O}_2 \text{ m}^{-3}$ for (a) weakly anti-estuarine and (b) estuarine circulations. Note the expanded vertical scale above 500 m.

4.2. Export Production and Sediment Fluxes

The seasonal cycle of the export productivity averaged over the eastern basin is shown in Figure 8 for each circulation; this export flux is evaluated at 100 m and averaged over 20 years at the end of the low- and high-nutrient input periods. The seasonal variations are a consequence of physical processes and irradiance, since the river and atmospheric inputs of nutrients are kept constant over the year. For the anti-estuarine circulations, there is a convective transfer of nutrients from the nutricline to the euphotic zone, which results in a spring increase in export production. In addition, for the weakened anti-estuarine case, there is a secondary maximum in production during the autumn, again associated with the onset of convective overturning. However, in the estuarine circulation, the lack of buoyancy-driven convective mixing leads to little seasonal cycle in both the nutrient supply to the euphotic zone and export production.

The mean export production over the year for the strong anti-estuarine circulation is 0.3 and $0.6 \text{ mol C m}^{-2} \text{ yr}^{-1}$ for the low- and high-nutrient input scenarios, respectively (Table 3). The export production increases slightly to $0.7 \text{ mol C m}^{-2} \text{ yr}^{-1}$ for the weakened anti-estuarine circulation owing to higher nutrient concentrations in the nutricline. The export production for the estuarine case reaches $1 \text{ mol C m}^{-2} \text{ yr}^{-1}$ owing to the upwelling of nutrient-rich waters.

The geographical distribution of export production for the three circulations at the end of the high-nutrient input period is shown in Figure 9. For the strong anti-estuarine model, areas of high production ($> 1 \text{ mol C m}^{-2} \text{ yr}^{-1}$) are localized near the coastline. Much of the Ionian and Levantine support very little productivity. In the weakened anti-estuarine case, while more production is supported on average, it is still concentrated near the coasts. However, in the estuarine case there is a striking increase in production away from

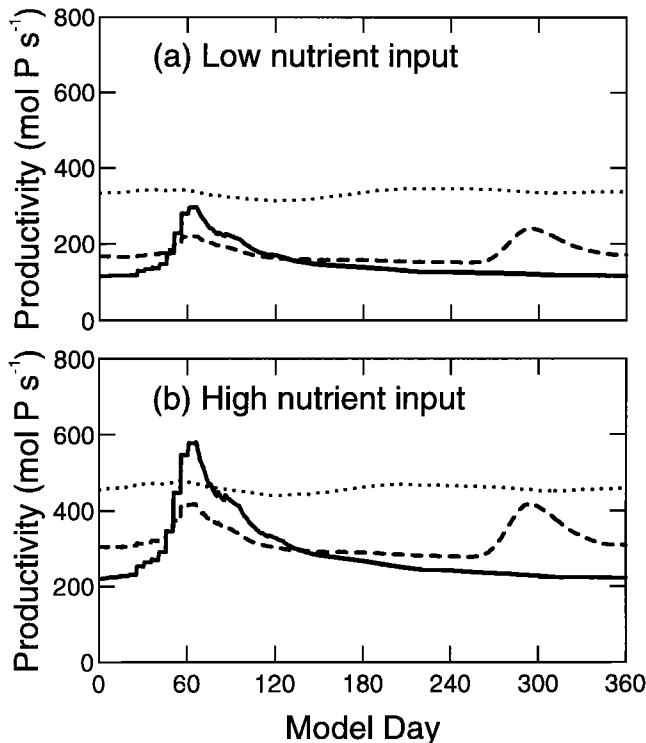


Figure 8. The seasonal cycle of modeled productivity integrated across the eastern basin. (a) The results for the three circulations with low-nutrient input at the end of 1000 years, and (b) with high-nutrient input at the end of 2000 years are shown. The solid line is the strong anti-estuarine case, the dashed line is the weakened anti-estuarine case, while the dotted line is the estuarine circulation.

the coastal regions which is driven by upwelling in some regions of the model, locally as high as $2\text{--}3 \text{ mol C m}^{-2} \text{ yr}^{-1}$. Note the strong dipole structure at 27°E which is related to regions of predominantly cyclonic circulation (upwelling) in the north and anticyclonic circulation (down-welling) in the south; the exact position of these features depends upon the wind forcing and topography.

The strong anti-estuarine circulation remains well ventilated so no significant deposition occurs in the model. Figure 10 shows the geographic distribution of preservation at the sea floor, again at the end of the high-nutrient input period. The weakened anti-estuarine case shows significant areas of deposition, particularly in the marginal basins and near coastlines. However, deposition is more widespread in the estuarine case, exceeding $0.5 \text{ mol C m}^{-2} \text{ yr}^{-1}$ in the marginal basins. The results are summarized in Table 3.

5. Discussion

5.1. Overview

Observational evidence suggests that episodes of sapropel formation are associated with enhanced export production and/or suboxic deep water. This modeling study investigates the role of the thermohaline circulation in both these processes in the eastern Mediterranean. The model results are relevant to the issue of sapropel formation in general, although the quantitative predictions, particularly for the weakened anti-estuarine case, are most valid for S_1 for which the model forcing is known to be appropriate.

5.2. Mechanisms for Sapropel Formation

The model study shows that increasing the buoyancy input over the eastern Mediterranean reduces the ventilation of the deep waters and increases the stratification of the upper ocean. If there is sufficient buoyancy input, then the sense of the thermohaline circulation can reverse from the present-day anti-estuarine circulation to an estuarine circulation. Given the major uncertainties in estimating the buoyancy forcing (from reconstructions of surface temperature or salinity), it is important to be able to identify characteristic observable signals for each type of circulation.

This study suggests that the weakened anti-estuarine and estuarine circulations differ in that (1) there are higher levels of export production in the estuarine circulation given the same atmospheric and river inputs of nutrients and (2) anoxia extends up to surface waters (below a thin mixed layer) for

Table 3. Summary of Observed and Model Export Production, Anoxia, and Sediment Fluxes

	Export Production, $\text{mol C m}^{-2} \text{ yr}^{-1}$	Suboxia/Anoxia	Maximum Sediment Flux, $\text{mol C m}^{-2} \text{ yr}^{-1}$
Present Day (Observed)	0.5–1.0	no	nil
Present Day (Model)	0.3–0.6	no	nil
Weak Anti-Estuarine	0.4–0.7	below $\sim 500 \text{ m}$	0.1–0.2
Weak Estuarine	0.7–1.0	below $\sim 100 \text{ m}$	0.5–1.0

Export production ($\text{mol C m}^{-2} \text{ yr}^{-1}$) averaged across the eastern Mediterranean taken from observation [Bethoux, 1989] and from the different model integrations (low- and high-nutrient input cases). Widespread anoxia and significant sediment fluxes occur in the model for the weakened anti-estuarine and estuarine circulations, but not for the strong anti-estuarine (present day) circulation.

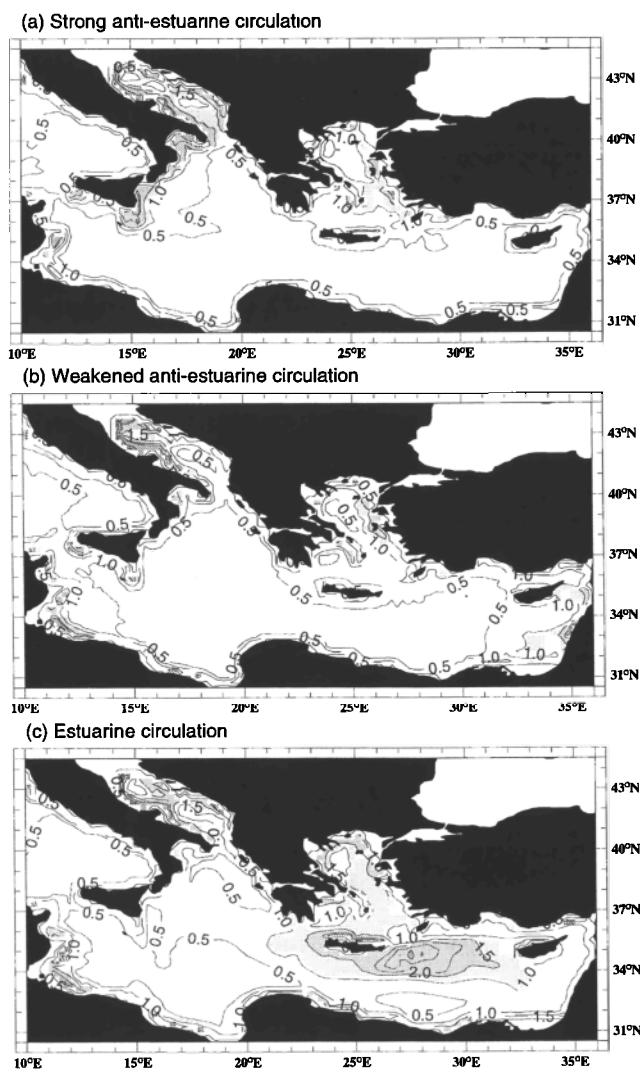


Figure 9. Annual export production for the three circulations at the end of the high nutrient input period. The contour interval is $0.5 \text{ mol C m}^{-2} \text{ yr}^{-1}$. The shaded areas highlight regions of export productivity greater than $1 \text{ mol C m}^{-2} \text{ yr}^{-1}$.

the estuarine case alone. Hence, near surface anoxia, as found for the Pliocene event by *Passier et al.* [1999], is consistent with an estuarine circulation. High levels of export production are confined to coastal regions in the anti-estuarine case, and the model suggests that very large increases in external nutrient input would be required to drive anoxia. In contrast, high values of export production in the interior of the basin occur in the estuarine circulation, particularly in cyclonic gyres.

Recently, *Kemp et al.* [1999] have brought to light the role of mat-forming diatoms in Mediterranean sapropels, recording export production of $7\text{--}14 \text{ mol C m}^{-2} \text{ yr}^{-1}$ for S_5 . The mat-forming diatoms are associated with high stratification and can vertically migrate to access nutrients in the nutricline [*Villareal et al.*, 1993]. However, the diatoms can only

be part of the answer, since this high export flux would exhaust the inorganic nutrients in the nutricline unless there were a compensating supply of new nutrients. For example, the equivalent organic phosphorus export flux is of the order of $0.1 \text{ mol P m}^{-2} \text{ yr}^{-1}$ (assuming a standard Redfield ratio) which would exhaust a phosphate concentration of $0.001 \text{ mol P m}^{-3}$ over the upper 500 m (see profile in Figure 6) in roughly 5 years. The high stratification is indicative of a local surface buoyancy input, but this signal may be associated with either a anti-estuarine or estuarine circulation. Consequently, the nutrients needed for the organic carbon export for S_5 have either to be fluxed into the upper ocean by upwelling or through much enhanced river run-off or atmospheric deposition.

5.3. The Holocene and S_1

Modeling studies by *Myers et al.* [1998] demonstrate that different salinity reconstructions for the Holocene all give rise to a weakened, shallower version of the present day anti-estuarine circulation, rather than an estuarine circulation. Hence, the model integration that is most appropriate for S_1 is the weakened, anti-estuarine case together with a factor 3 increase in river inputs of nutrients (over the preanthropogenic state) appropriate for the early Holocene [*Kallel et al.*, 1997].

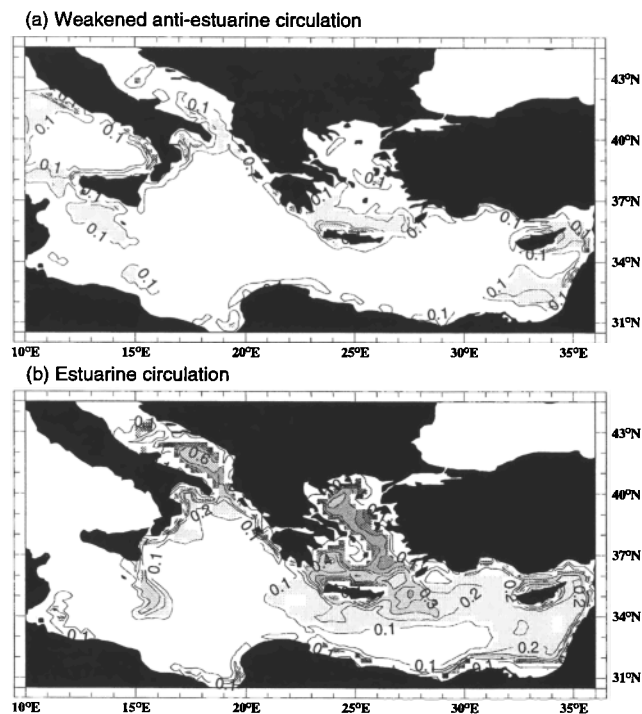


Figure 10. Annual flux of organic matter at the sea floor for (a) the weakened anti-estuarine circulation and (b) the estuarine circulation with the high-nutrient input. The contour interval here is $0.1 \text{ mol C m}^{-2} \text{ yr}^{-1}$. The shaded regions also highlight deposition greater than $0.1 \text{ mol C m}^{-2} \text{ yr}^{-1}$.

The model predicts that organic carbon is preserved via suboxic or anoxic conditions below the surface waters. The anoxia first occurs at mid-depth after around 1000 model years (given the initial conditions) and then advances to the deeper waters by 1500 years. Accordingly, carbon deposits should first form at mid-depths then spread to the deeper waters. However, this advance may be more rapid in the model than can be resolved by geochemical dating [cf. *Strohle and Krom, 1997*].

The organic carbon flux at the sea floor for S_1 is estimated to be in the range $0.2 \text{ mol C m}^{-2} \text{ yr}^{-1}$ [*Calvert et al., 1992*] to $1 \text{ mol C m}^{-2} \text{ yr}^{-1}$ [*Howell and Thunell, 1992*]. The modeled flux of organic material at the sea floor is close to the lower estimate ($0.2 \text{ mol C m}^{-2} \text{ yr}^{-1}$) in parts of the open ocean, but only exceeds $0.3 \text{ mol C m}^{-2} \text{ yr}^{-1}$ near the coasts and in the marginal basins. Note that the present model assumes that phosphorus remains the limiting nutrient for this climate regime in the eastern Mediterranean. However, higher river transport of phosphate may cause a reversion to nitrogen limitation, in which case the model estimates must be considered as lower limits. A high estimate of Holocene productivity led *Howell and Thunell [1992]* to invoke an estuarine circulation in the eastern Mediterranean. However, this hypothesis is inconsistent with modeling by *Myers et al. [1998]* using palaeoceanographic salinity reconstructions. In addition, lack of evidence for widespread near-surface anoxia in the Holocene is also consistent with the weakened anti-estuarine model. Taken together, the model results suggest that sapropel S_1 is formed by a combination of increased production (from enhanced river input of nutrients and a change in nutrient transports) and enhanced preservation of organic matter (as a result of reduced deep water ventilation and the formation of suboxic conditions).

6. Conclusion

The thermohaline circulation influences the formation of sapropels in the eastern Mediterranean by modulating the supply of nutrients to the euphotic zone and controlling the extent of anoxia. This study compares the biogeochemical signals associated with a weakening of the present day thermohaline circulation and a more dramatic reversal of the thermohaline circulation. Sapropels can be formed in both cases, so it is important to be able to distinguish between the circulations from observable signals. These modeling results suggest that for a weakening of the present day circulation, there is only a modest increase in productivity and the anoxia extends up to the base of the dense water outflow for the basin. However, the model indicates that a weakened anti-estuarine circulation can provide enough deposition of organic carbon to form, for example, the S_1 sapropel which has a relatively low organic carbon content. In contrast, with a reversal of the circulation, there is a more dramatic increase in productivity which naturally leads to higher organic carbon content sediments. In addition, anoxia extends to the base of a shallow winter mixed layer, suggest-

ing anoxic or sulphidic near-surface water is a good diagnostic for an estuarine circulation.

Appendix: Phosphate Model Parameters

The behavior of the simple model based on phosphate, detritus, and oxygen described in section 3 is controlled by the boundary conditions imposed at the surface, together with two main parameters: the phosphate utilization rate in the euphotic zone and the remineralization rate in the deep ocean. The choice of model parameters and the surface input of phosphate are now examined more closely.

A1. Phosphate Utilization Rate

Phosphate in the surface layers of the model is utilized at a rate λ which represents the light-limited uptake of nutrients by phytoplankton in (2). The timescale $1/\lambda$ gives a measure of the residence time for phosphate in the surface layers. The maximum rate in the present model corresponds to $1/\lambda \sim 4$ weeks following *Najjar et al. [1992]* and *Williams and Follows [1998]*. The maximum rate is modulated by the seasonal cycle in insolation [*Paltridge and Platt, 1976, Chapter 3*] and decreases exponentially with depth assuming the extinction coefficient of 0.05 m^{-1} for the light intensity.

A2. Remineralization Rate

The remineralization rate for detritus in the model, r , together with the sinking speed, w_s , control the quantity of detritus which survives to reach the sea floor (at a given depth). For this simple model, it is useful to define a remineralization e -folding depth scale $z^* = w_s/r$.

In a well-oxygenated water column a very small percentage of detritus making up export production is observed to survive to reach the sea floor. In the eastern Mediterranean (typically 3000 m), of order 0.1% of organic material will survive in well-oxygenated regions [*Howell and Thunell, 1992*]. This gives an e -folding depth of $z^* \sim 450$ m, consistent with estimates from sediment traps [e.g., *Martin et al., 1987*].

However, in an oxygen-poor water column, remineralization is slower and more material survives to the sea floor. Palaeoceanographic studies [*Kemp et al., 1999*] and present day Black Sea studies [*Arthur et al., 1994*] suggest around 5–10% preservation. The means the remineralization rate is roughly 3 times slower ($z^* \sim 1350$ m) than for the oxygenated case, which is consistent with laboratory experiments examining bacterial action in oxic and anoxic conditions [*Harvey et al., 1995*].

The model remineralization rate is determined by fixing w_s to be 200 m d^{-1} [e.g., *Smith, 1989; Honjo and Mangani, 1993; Smith et al., 1996*] and setting z^* to 450 m. With the onset of suboxic conditions, taken to be at $0.06 \text{ mol O}_2 \text{ m}^{-3}$ [*Rosenburg, 1980*], the remineralization rate is linearly reduced to one third of this value at zero oxygen concentration. In this way, the fraction of material reaching

the sea floor in the model is consistent with the observational estimates.

A3. Surface Phosphate Flux

Best estimates of river input of phosphate for the Mediterranean as a whole before anthropogenic pollution is taken into account are 40–60 mol s⁻¹ [McGill, 1969; Sarmiento *et al.*, 1988, and references therein]. Atmospheric fluxes contained in wind-blown dust and rainfall [Duce *et al.*, 1991] are observed to be 2–3 × 10⁻¹¹ mol m⁻² s⁻¹ for the Mediterranean area [Martin *et al.*, 1989; Migon *et al.*, 1989; Herut and Krom, 1996]. There is a large Saharan dust contribution in this region [e.g., Chester *et al.*, 1984] which is not strongly affected by pollution. Estimates for the current overall phosphate source, including river pollution, are around 360 mol s⁻¹ [e.g., Bethoux *et al.*, 1992].

The basic model configuration employs a river flux of 30 mol P s⁻¹ into both the eastern and western basins, uniformly distributed between all model grid cells contiguous with the coastline (the extent of one grid cell is about 20 km). A baseline atmospheric flux based on the above figures gives 20 mol P s⁻¹ in the western basin and 35 mol P s⁻¹ in the eastern basin, distributed uniformly across all model grid cells. For the eastern basin this gives a total nutrient supply of 65 mol P s⁻¹. For the higher nutrient input case it is assumed that a factor 3 increase in river run-off is accompanied by a commensurate increase in nutrient flux, while the atmospheric flux is unchanged. This gives a total of 125 mol P s⁻¹ for the eastern basin. This increase in fresh water run-off is consistent with estimates for the early Holocene [Kallel *et al.*, 1997].

Acknowledgments. This work was funded by the European Community MAST programme under MAS3-CT95-0043 (CLIVAMP) and MAS3-CT98-0189 (MEDNET). We are grateful for comments from Eelco Rohling and an anonymous reviewer as well as useful discussions with the CLIVAMP group, George Wolff, Roger Wilson, and Mike Krom.

References

- Arthur, M.A., W.E. Dean, E.D. Neff, B.J. Hay, J. King, and G. Jones, Valve calibrated records of carbonate and organic-carbon accumulation over the last 2000 years in the Black Sea, *Global Biogeochem. Cycles*, 8, 195–217, 1994.
- Berland, B.R., A.G. Benzhitski, Z.P. Burlakova, L.V. Georgieva, M.A. Izmetstieva, V.I. Kholodov, and S.Y. Maestrini, Conditions hydrologiques estivales en Méditerranée, répartition du phytoplancton et de la matière organique, *Oceanol. Acta*, 9, 163–177, 1988.
- Bethoux, J.P., Oxygen consumption, new production, vertical advection and environment evolution in the Mediterranean sea, *Deep Sea Res.*, 36, 769–781, 1989.
- Bethoux, J.P., P. Morin, C. Madec, and B. Gentili, Phosphorus and nitrogen behaviour in the Mediterranean Sea, *Deep Sea Res.*, 39, 1641–1654, 1992.
- Brasseur, P., J.M. Beckers, J.M. Brankart, and R. Schoenauen, Seasonal temperature and salinity fields in the Mediterranean Sea: Climatological analyses of an historical data set, *Deep Sea Res., Part 1*, 43, 159–192, 1996.
- Calvert, S.E., B. Nielsen, and M. R. Fontugne, Evidence from nitrogen isotope ratios for enhanced productivity during formation of eastern Mediterranean sapropels, *Nature*, 359, 223–225, 1992.
- Conkright, M.E., S. Levitus, and T.P. Boyer, *World Ocean Atlas 1994, NOAA Atlas NESDIS*, Vol. 1, 162 pp., U.S. Dept. Comm., Washington, D.C., 1994.
- Chester, R., E.J. Sharples, and G.S. Sandres, Saharan dust over the Tyrrhenian Sea, *Atmos. Environ.*, 18, 101–123, 1984.
- Duce, R.A., et al., The atmospheric input of trace species to the world ocean, *Global Biogeochem. Cycles*, 5, 193–259, 1991.
- Gent, P.R., and J.C. McWilliams, Isopycnal mixing in ocean circulation models *J. Phys. Oceanogr.*, 20, 150–155, 1990.
- Haines, K., and P. Wu, A modelling study of the thermohaline circulation of the Mediterranean Sea: water formation and dispersal, *Oceanol. Acta*, 18, 401–417, 1995.
- Haney, R.L., Surface thermal boundary condition for ocean circulation models, *J. Phys. Oceanogr.*, 1, 241–248, 1971.
- Harvey, H.R., J.H. Tuttle, and J.T. Bell, Kinetics of phytoplankton decay during simulated sedimentation: Changes in biochemical composition and microbial activity under oxic and anoxic conditions, *Geochim. Cosmochim. Acta*, 59, 3367–3377, 1995.
- Herut, B., and M.D. Krom, Atmospheric input of nutrients and dust to the SE Mediterranean, in *The Impact of Desert Dust Across the Mediterranean*, edited by S. Guerzoni and R. Chester, pp. 349–358, Kluwer Acad., Norwell, Mass., 1996.
- Hewitt, C.D., and J.F.B. Mitchell, A fully coupled GCM simulation of the climate of the mid-Holocene, *Geophys. Res. Lett.*, 25, 361–364, 1998.
- Honjo, S., and S.J. Manganini, Annual biogenic particle fluxes to the interior of the North Atlantic Ocean: Studied at 34°N 21°W and 48°N 21°W, *Deep Sea Res., Part II*, 40, 587–607, 1993.
- Howell, M.W., and R.C. Thunell, Organic carbon accumulation in Bannock Basin: Evaluating the role of productivity in the formation of eastern Mediterranean sapropels, *Mar. Geol.*, 103, 461–471, 1992.
- Kallel, N., M. Paterne, J.-C. Duplessy, C. Vergnaud-Grazzini, C. Pujol, L. Labeyrie, M. Arnold, M. Fontugne, and C. Pierre, Enhanced rainfall in the Mediterranean region during the last sapropel event, *Oceanol. Acta*, 20, 697–712, 1997.
- Kemp, A.E.S., R.B. Pearce, I. Koizumi, J. Pike, and S.J. Rance, The role of mat-forming diatoms in the formation of Mediterranean sapropels, *Nature*, 398, 57–61, 1999.
- Killworth, P.D., D. Staniforth, D.J. Webb, and S.M. Patterson, The development of a free-surface Bryan-Cox-Semtner ocean model, *J. Phys. Oceanogr.*, 21, 1333–1348, 1991.
- Krom, M.D., N. Kress, S. Brenner, and L.I. Gordon, Phosphorus limitation of primary productivity in the eastern Mediterranean Sea, *Limnol. Oceanogr.*, 36, 424–432, 1991.
- Liss, P.S., and L. Merlivat, Air-sea gas exchange rates: introduction and synthesis, in *The Role of Air-Sea Exchange in Geochemical Cycling*, edited by P. Baut-Ménard, pp. 113–127, D. Reidel, Norwell, Mass., 1986.
- Mangini, A., and P. Schlosser, The formation of eastern Mediterranean sapropels, *Mar. Geol.*, 72, 115–124, 1986.
- Martin, J.H., G.A. Knauer, D.M. Karl, and W.W. Broenkow, VERTEX: Carbon cycling in the northeast Pacific, *Deep Sea Res.*, 34, 267–285, 1987.
- Martin, J.-M., F. Elbaz-Poulichet, C. Guieu, M.-D. Loje-Pilot, and G. Han, River versus atmospheric Input of Material to the Mediterranean Sea: An overview, *Mar. Chem.*, 28, 159–182, 1989.
- McGill, D.A., A budget for dissolved nutrient salts in the Mediterranean Sea, *Cah. Océanogr.*, 21, 543–554, 1969.
- Migon, C., G. Copin-Montegut, L. Élegant, and J. Morelli, Étude de l'apport atmosphérique en sels nutritifs au milieu côtier Méditerranéen et implications biogéochimiques, *Oceanol. Acta*, 12, 187–191, 1989.

- Myers, P.G., and K. Haines, Seasonal and interannual variability in a model of the Mediterranean under flux forcing, *J. Phys. Oceanogr.*, in press, 2000.
- Myers, P.G., K. Haines, and E.J. Rohling, Modelling the paleocirculation of the Mediterranean: The last glacial maximum and the Holocene with emphasis on the formation of sapropel S₁, *Paleoceanography*, *13*, 586–606, 1998.
- Najjar, R.G., Simulations of the phosphorus and oxygen cycles in the world ocean using a general circulation model, Ph.D. thesis, Princeton Univ., Princeton, N.J., 1990.
- Najjar, R.G., J.L. Sarmiento, and J.R. Toggweiler, Downward transport and fate of organic matter in the ocean: simulations with a general circulation model, *Global Biogeochem. Cycles*, *6*, 45–76, 1992.
- Paltridge, G.W., and C.M.R. Platt, *Radiative processes in Meteorology and Climatology*, Elsevier Sci., New York, 1976.
- Passier, H.F., H.-J. Bosch, I.A. Nijenhuis, L.J. Lourens, M.E. Böttcher, A. Leenders, J.S. Sinninghe Damsté, G.J. de Lange, and J.W. de Leeuw, Sulphidic Mediterranean surface waters during Pliocene sapropel formation, *Nature*, *397*, 146–149, 1999.
- Pinardi, N., and A. Navarra, Baroclinic wind adjustment processes in the Mediterranean Sea, *Deep Sea Res., Part II*, *40*, 1299–1326, 1993.
- Redfield, A.C., B.H. Ketchum, and F.A. Richards, The influence of organisms on the composition of sea water, in *The Sea*, vol. 2, edited by M.N. Hill, pp. 26–76, Wiley-Interscience, New York, 1963.
- Roether, W.R., B. Manca, B. Klien, D. Bregant, and D. Georgopoulos, Eastern Mediterranean deep waters found in an entirely new state, *Science*, *271*, 333–335, 1996.
- Rohling, E.J., Review and new aspects concerning the formation of eastern Mediterranean sapropels, *Mar. Geol.*, *122*, 1–28, 1994.
- Rohling, E.J., and W.W.C. Gieskes, Late Quaternary changes in Mediterranean intermediate water density and formation rate, *Paleoceanography*, *4*, 531–545, 1989.
- Rosenburg, R., Effect of oxygen deficiency on benthic macrofauna in fjords, in *Fjord Oceanography*, edited by H.J. Freeland, D.M. Farmer, and C.D. Levings, pp. 499–514, Plenum, New York, 1980.
- Roussenov, V., E. Stanev, V. Artale, and N. Pinardi, A seasonal model of the Mediterranean Sea general circulation, *J. Geophys. Res.*, *100*, 13,515–13,538, 1995.
- Sancetta, C., Mediterranean sapropels: Seasonal stratification yields high production and carbon flux, *Paleoceanography*, *9*, 195–196, 1994.
- Sarmiento, J.L., T. Herbert, and J.R. Toggweiler, Mediterranean nutrient balance and episodes of anoxia, *Global Biogeochem. Cycles*, *2*, 427–444, 1988.
- Smith, C.R., D.J. Hoover, S.E. Doan, R.H. Pope, D.J. Demaster, F.C. Dobbs, and M.A. Altabet, Phytodetritus at the abyssal sea floor across 10° of latitude in the central equatorial Pacific, *Deep Sea Res., Part II*, *43*, 1309–1338, 1996.
- Smith, K.L., Short time-series measurements of particulate organic carbon flux and sediment community oxygen consumption in the North Pacific, *Deep Sea Res.*, *36*, 1111–1119, 1989.
- Stratford, K., Flux-limited advection for tracers in an ocean general circulation model, *J. Atmos. Ocean Tech.*, *16*, 1284–1290, 1999.
- Stratford, K., R.G. Williams, and P.G. Drakopoulos, Estimating climatological age from a model-derived oxygen–age relationship in the Mediterranean, *J. Mar. Syst.*, *18*, 215–226, 1998.
- Strohle, K., and M.D. Krom, Evidence for the evolution of an oxygen minimum layer at the beginning of S-1 sapropel deposition in the eastern Mediterranean, *Mar. Geol.*, *140*, 231–236, 1997.
- Takahashi, T., W.S. Broecker, and S. Langer, Redfield ratio based on chemical data from isopycnal surfaces, *J. Geophys. Res.*, *90*, 6907–6924, 1985.
- Thuburn, J., Multidimensional flux-limited advection schemes, *J. Comput. Phys.*, *123*, 74–83, 1996.
- Thunell, R.C., and D.F. Williams, Glacial-Holocene salinity changes in the Mediterranean Sea in relation to the evolution of late neogene climates, *Nature*, *338*, 493–496, 1989.
- Villareal, T.R., M.A. Altabet, and K. Culver-Rymsza, Nitrogen transport by vertically migrating diatom mats in the North Pacific Ocean, *Nature*, *363*, 709–712, 1993.
- Weiss, R.F., The solubility of nitrogen, oxygen and argon in water and seawater, *Deep Sea Res.*, *17*, 721–735, 1970.
- Williams, R.G., and M.J. Follows, The Ekman transfer of nutrients and maintenance of new production over the North Atlantic, *Deep Sea Res.*, *45*, 461–489, 1998.

P.G. Myers, Department of Physics and Physical Oceanography, Memorial University of Newfoundland, St. John's, Newfoundland A1B 3X7, Canada. (myers@physics.mun.ca)

K. Stratford, Department of Meteorology, University of Edinburgh, The King's Buildings, Mayfield Road, Edinburgh EH9 3JZ, UK. (kevin@met.ed.ac.uk)

R.G. Williams, Oceanography Laboratories, Bedford St. North, University of Liverpool, Liverpool L69 3BX, UK. (ric@liv.ac.uk)

(Received March 15, 1999; revised November 10, 1999; accepted November 18, 1999.)